Electrocatalytic synthesis of hydrogen peroxide on Au-Pd nanoparticles: from fundamentals to continuous production

Enrico Pizzutilo[a*], Olga Kasian[a], Chang Hyuck Choi[a,b], Serhiy Cherevko[a,c], Graham J. Hutchings[d], Karl J. J. Mayrhofer[a,c,e] and Simon J. Freakley[d*]

[a]*Department of Interface Chemistry and Surface Engineering, Max-Planck-Institut für Eisenforschung GmbH, Max-Planck-Strasse 1, 40237 Düsseldorf, Germany*

[b]*School of Materials Science and Engineering, Gwangju Institute of Science and Technology, Gwangju 61005, Republic of Korea*

[c]*Helmholtz-Institute Erlangen-Nürnberg for Renewable Energy (IEK-11), Forschungszentrum Jülich, Egerlandstr. 3, 91058 Erlangen, Germany*

[d]*Cardiff Catalysis Institute, School of Chemistry, Cardiff University, Main Building, Park Place, Cardiff, CF10 3AT*

[e]*Department of Chemical and Biological Engineering, Friedrich-Alexander-Universität Erlangen-Nürnberg, Egerlandstr. 3, 91058 Erlangen, Germany*

[*]*Corresponding authors: pizzutilo@mpie.de*, *freakleys@cardiff.ac.uk*

Abstract

The electrochemical synthesis of hydrogen peroxide (H_2O_2) represents a promising alternative to the anthraquinone process, as it combines on-site chemical and electrical production. The design of selective electrocatalysts is challenging and is commonly based on the alloying of elements to generate a synergistic effects and increase activity. In the present work, we report the electrochemical activity of Au-Pd nanoparticles immobilized directly onto an electrode as a model to study H_2O_2 electrochemical synthesis from fundamentals to continuous production. The impact of composition on the oxygen reduction (ORR), on the selectivity, as well as the peroxide reduction and oxidation (PROR) are studied.

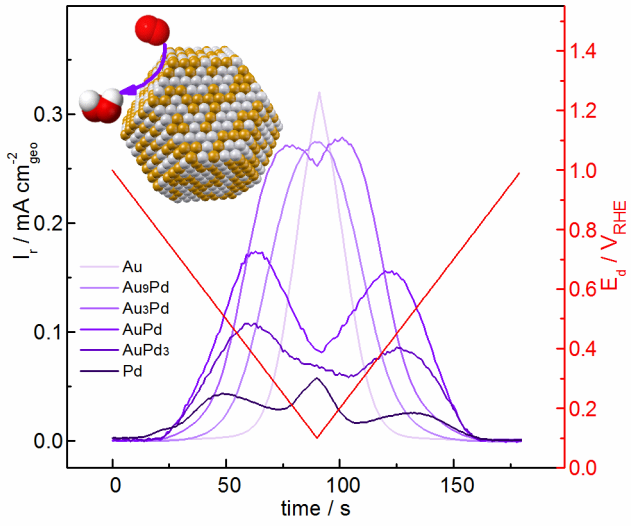

Keywords: gold, palladium, hydrogen peroxide, electrocatalyst

1 Introduction

Hydrogen peroxide (H_2O_2) is an excellent green oxidant applied in several important processes, for instance pulp and paper bleaching, water-cleaning, disinfection and industrial synthesis of consumer goods [1, 2]. At present, H_2O_2 is manufactured almost exclusively through the anthraquinone process in centralized reactors, where it is often concentrated up to 70 wt% to reduce costs [3]. However, as typical end-users require concentrations of 2-8 wt% [2], local production by means of a less energy demanding synthetic technology is desirable [4].

Electrochemical reactors represent an attractive alternative for the production of H_2O_2 via O_2 reduction on-site. Intensive research has been carried out over recent years both in alkaline [5, 6] and acidic medium [7-9]. However, as H_2O_2 degradation can be base catalysed, more promising is the synthesis in acidic medium [10]. In acid, H_2O_2 is synthesized from O_2 and protons in a 2-electron ORR pathway ($O_{2(g)} + 2H^+_{(aq)} + 2e^- \rightarrow H_2O_{2(aq)}$) [11]; its standard potential is 0.69 V [12]. The well-developed technology of proton exchange membrane fuel cells (PEM-FC) could be directly utilized for eventual H_2O_2 production and collection of electrical current on a larger scale.

Noble metals such as Pt and Pd are the most promising PEM-FC catalysts, due to their high stability at potentials of operational interest in acidic environments [12]. However, both tend to reduce O_2 to H_2O in a 4-electron pathway with high faradaic efficiencies [11]. Recently, the addition of mercury to Pt or Pd led to the discovery of unprecedentedly active electrocatalyst for the H_2O_2 synthesis, which was ascribed to the synergetic presence of two metals with different oxygen binding energies [8, 13]. However, the toxicity of Hg might ultimately limit the application of these alloys. Au and Au-Pd catalysts were shown to have the lowest overpotential besides Hg-based catalysts [8]. Au and Pd are safe and, thanks to their high dissolution onset-potential, also promising candidates in acidic media [14]. In addition AuPd nanoparticles supported on carbon and oxide materials have been extensively studied as heterogeneous catalysts for direct H_2O_2 synthesis from molecular H_2 and O_2 [15].

Pd binds oxygen intermediates strongly and has a low ORR overpotential close to Pt [16]. Au shows remarkable variation in the kinetics and the mechanism of the ORR varying between 2- and 4-electrons process, depending on support, crystallographic orientation, size and pH [17-19]. Such behavior is common to all electrodes that interact weakly with O_2 (i.e. Au, Ag, Hg) [17, 20]. The alloy of Au and Pd, has been shown to influence activity and selectivity for the ORR [7, 21, 22]. Jirkovsky *et al.* studied the influence of carbon supported Au-Pd catalysts (Pd < 50%) and showed that the addition of a small fraction (8%) of Pd leads to an increase in H_2O_2 selectivity compared to pure Au [7]. This was attributed to the ensemble (or geometric) effect caused by the presence of finely dispersed Pd in Au, influencing the O_2 adsorption on the catalyst surface [23]. Erikson *et al.* studied the ORR behavior of Au-Pd electrodeposited catalysts with higher Pd% (only Pd > 50%) however particle size distributions were variable between samples [22].

In this context, we studied the performance of colloidal AuPd nanoparticles immobilized directly onto an electrode over a wide range between pure Au and Pd (Au, Au_9Pd, Au_3Pd, AuPd, $AuPd_3$, Pd) and with controlled particle size distributions around 3-4 nm (statistical size from TEM micrographs). In particular, we present their ORR activity, H_2O_2 selectivity and the PROR in an acidic environment with the rotating ring-disc electrode (RRDE). Finally, potentiostatic production of H_2O_2 (2 and 30 min) provides us additional information on the catalyst behavior in real systems.

2 Materials and Methods

2.1 Nanoparticle synthesis and characterization

For the preparation of Au-Pd nanoparticles a colloidal synthesis method described elsewhere was followed [24]. An aqueous solution (800 ml, HPLC grade water) containing metal precursors in the desired ratio was prepared from stock solutions of $PdCl_2$ (6 mg_{Pd} ml^{-1}, Sigma Aldrich, Reagent Plus® 99%) and $HAuCl_4 \cdot 3H_2O$ (12.5 mg_{Au} ml^{-1} Sigma Aldrich, Au assay ≥49.0%) with a total metal content of 20 mg metal in 800 ml. Separately aqueous solutions of $NaBH_4$ (Sigma Aldrich, 0.1 M) and Poly(vinyl alcohol) (PVA) (1 wt% aqueous solution, Sigma Aldrich, MW=10,000, 80% hydrolyzed) were also prepared. PVA addition to the metal solution (PVA/(Au + Pd) (w/w)=1.2) was followed by addition of a freshly prepared solution of $NaBH_4$ (0.1 M, $NaBH_4$/(Au + Pd) (mol/mol)=5) to form a dark-brown sol which is generated in 30 min. The obtained solutions were finally concentrated with the help of a rotary evaporator to 0.1 mg ml^{-1}.

For examination by scanning transmission electron microscopy (STEM), to determine the particle size distributions, a JEOL 2200FS TEM operating at 200 kV was used. The prepared solutions were dispersed onto a lacey carbon film supported by a gold TEM grid and then subjected to bright field contrast.

The Au:Pd molar ratios were measured by ICP-MS (NexION 300X, Perkin Elmer) by dissolving the AuPd samples in boiling aqua regia (4 ml solution, Merck Suprapur acids).

XPS measurements were performed applying a monochromatic Al Kα X-ray source (1486.6 eV) operating at 15 kV and 25 W (Quantera II, Physical Electronics, Chanhassen). Analysis of the spectra was carried out using Casa XPS (http://www.casaxps.com/).

2.2 Electrochemical characterization

All electrochemical results were obtained via thin-film technique either on a rotating disc electrode (RDE, Ar background and PROR) or rotating ring–disc electrode (RRDE) method. Experiments were carried out at room temperature (≈24°C) in a three electrode Teflon cell and potentials refers to the reversible hydrogen electrode (RHE), measured prior to experiments. Mirror polished poly-Pt, poly-Au, poly-Pd (5 mm, MaTeck) and Au-Pd catalysts (10 μg_{metal} cm^{-2}) on glassy carbon (GC) with an area of 0.196 cm^2 were alternated as working electrodes. Both the counter electrode, a graphite rod, and the reference electrode, a saturated Ag/AgCl electrode (Metrohm), were separated by a Nafion membrane (Tschurl modification). Potentiostat (Gamry Reference 600) and rotator (MSR Pine Rotator System) were controlled with a Gamry V6 Software. The supporting electrolyte was gas (Ar or O_2) purged 0.1 M $HClO_4$, prepared by dilution of

concentrated perchloric acid (Suprapur®, Merck) in ultrapure water (PureLab Plus system, Elga, 18 MΩ-cm). For PROR, 10 mM H_2O_2 (AnalaR NORMAPUR) were added to the Ar purged electrolyte. More details about the single electrochemical method are available in the SI.

3 Results and discussion

3.1 TEM and Surface Characterization

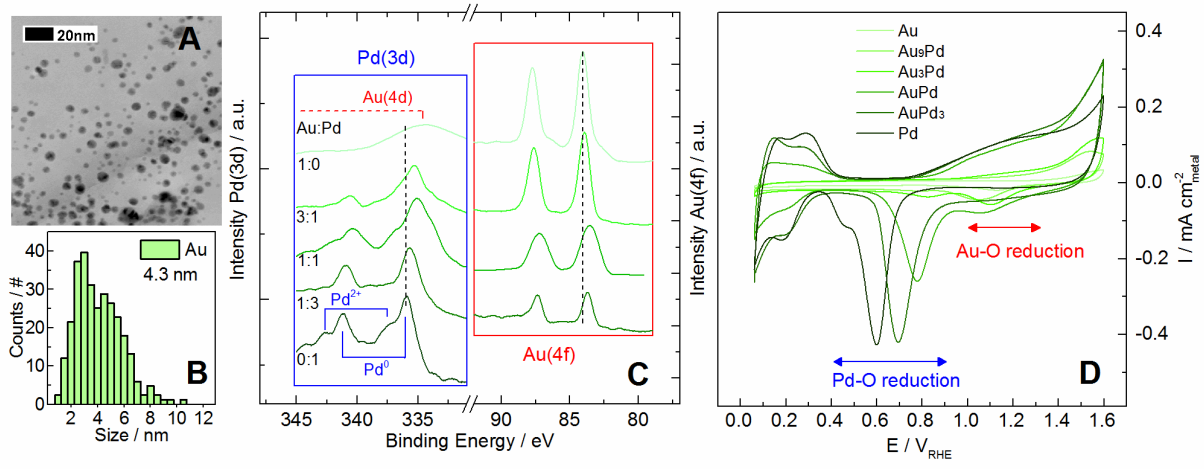

Figure 1 (a) Representative bright field TEM micrograph and (b) statistic particle size distribution of Au colloidal nanoparticles deposited on a lacey carbon TEM grid. The micrographs of the other prepared catalysts are shown in the SI. (c) XPS spectra for the series of freshly prepared Au-Pd catalysts and (d) corresponding initial cyclic voltammograms [0.1-1.6] V_{RHE} in Ar purged 0.1M $HClO_4$. Scan rate: 200 mV s^{-1}.

The Au-Pd nanoparticles (Au, Au_9Pd, Au_3Pd, AuPd, $AuPd_3$, Pd) are prepared through a sol-immobilization method yielding the presence of a face-centered cubic (fcc) structure, as recently described [24]. The average particle size and size distribution are estimated statistically from bright field STEM micrographs (Figure 1a-b and Figure S1.1-5). The sizes are summarized in Table 1 along with the Au:Pd molar ratios estimated with ICP-MS and XPS (Figure 1c). XPS spectra (Figure 1c) show a shift in Au 4f photoelectron peak towards lower binding energies once Pd is present, which is a typical feature observed for Au-Pd alloys [25]. The molar ration of the Au_9Pd estimated by XPS differs slightly from the value obtained via ICPMS. For low Pd content the estimation of the molar ratio with XPS is less accurate owing to direct overlap between Pd(3d) and Au(4d) peaks.

Table 1 Particle size and Au:Pd molar ratios estimated via ICP-MS and XPS of the prepared catalysts.

	N of particle	median / nm	st. dev.	Au:Pd ratio ICPMS	Au:Pd ratio XPS
Au	298	4.3	±1.3	100:0	100:0
Au_9Pd	362	2.7	±1.0	91:9	98:2
Au_3Pd	322	3.5	±1.1	77:23	74:26
AuPd	251	4.1	±0.8	46:54	48:52
$AuPd_3$	285	3.7	±1.1	26:74	27:73
Pd	277	3.2	±1.2	0:100	0:100

The shape of the initial Ar background cyclic voltammograms (CVs) (Figure 1d and as reference poly-Au and poly-Pd electrodes in Figure S2.1-2) are related to the surface state and composition. The upper potential limit (UPL) of 1.6 V_{RHE} is chosen in order to measure the Au oxide (denoted as Au-O due to lack of information about stoichiometry) reduction peak which is only distinguishable with high UPLs [26]. Typical features of Au and Pd vary with the composition. Hydrogen under potential deposition (H_{UPD}) is only present in samples with high Pd content (from 1:1 molar ratio Au:Pd onwards). Furthermore, two peaks in the H_{UPD} are observed for $AuPd_3$ and Pd in accordance with previous literature [27]. Proceeding anodically, the onset potential for the Pd oxide (Pd-O is used as exact composition is not known) and Au-O formation are around 0.7 V_{RHE} and 1.3 V_{RHE} respectively. The cathodic scan is dominated by two main features, namely Au-O and Pd-O reductions. For pure Pd and Au catalysts the maxima of the respective reduction peak were measured at 0.6 V_{RHE} and 1.1 V_{RHE}. The presence of one or two reduction peaks reflects the composition: (i) for low Pd content (Au_9Pd) only the Au-O reduction is visible (as in [7]), whereas (ii) for high Pd content ($AuPd_3$) only the Pd-O reduction is present (as in [28]); (iii) for intermediate compositions (Au_3Pd and AuPd), instead, two peaks are observed. Interestingly, the Pd-O peak position shifts significantly when Pd is mixed to Au. Such a shift has been attributed to alloying [7, 22, 28] and was exploited by Rand and Woods to define the surface composition based on a linear dependence with the reduction potential [29]. However, this approach was shown to be limited only to high Pd content (> 40%) [28, 30] and for Au-Pd non-polarized to H_{UPD} where H absorption might take place [28]. Even though quantification is difficult, the position and the associated charges are good indicators of surface composition changes. Note, that also potential cycling might cause minor changes in surface composition due to metal segregation [21].

3.2 Oxygen Reduction Reaction (ORR)

The ORR on Au-Pd nanoparticles is studied with the RRDE (calibration in Figures S3.1-2) with simultaneous H_2O_2 monitoring at the ring during the ORR. From the detected currents, disc (I_d) and ring (I_r), the H_2O_2 selectivity ($S_{H_2O_2}$) is derived.

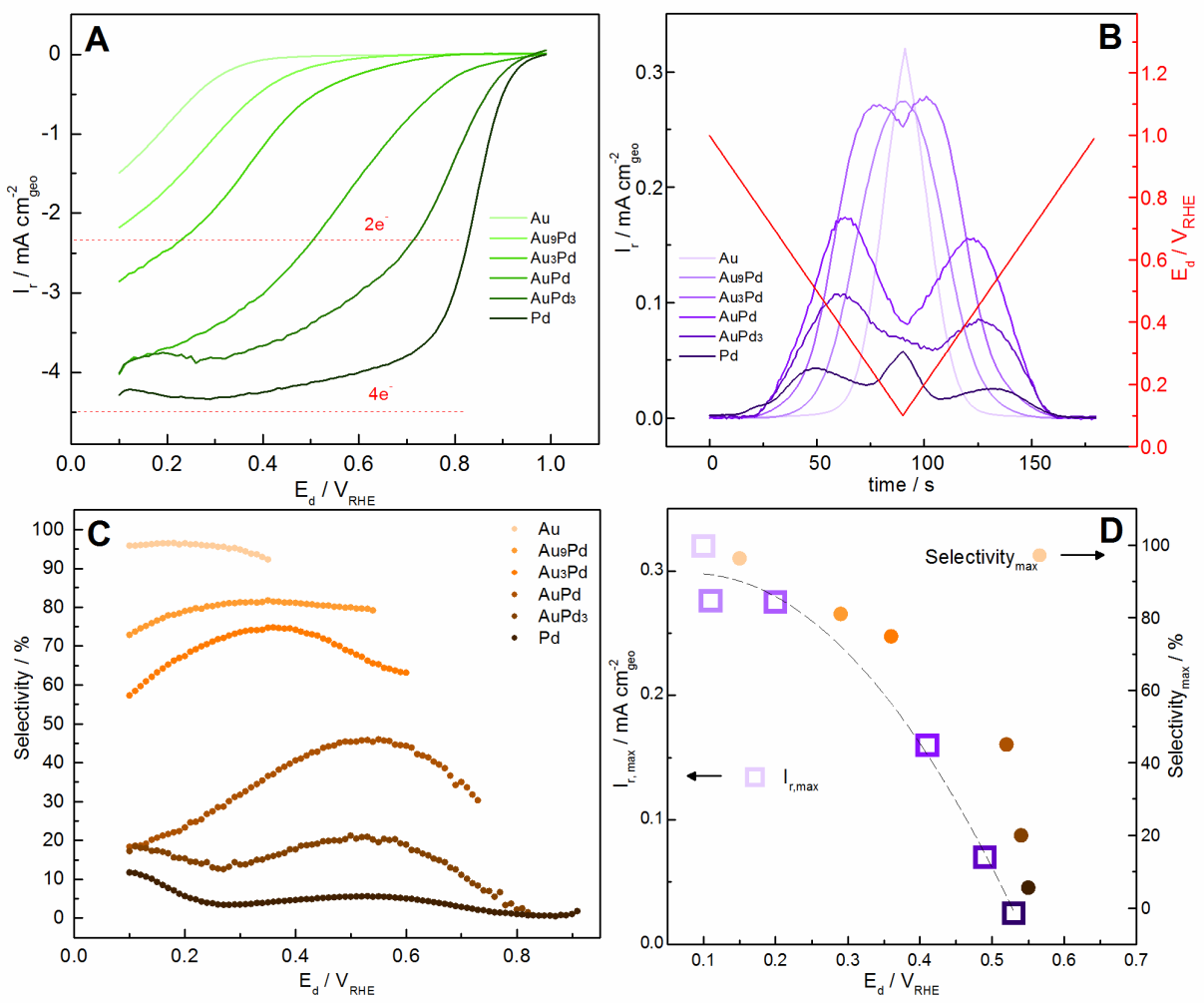

Figure 2 RRDE results obtained for ORR on different Au-Pd catalyst compositions in O_2 saturated 0.1M $HClO_4$. Rotation: 900 rpm. Scan rate: 50 mV s^{-1}. E_r: 1.28 V_{RHE}. The colors (green for I_d, violet for I_r, brown for S_{H2O2}) are graded with the change in composition. (a) Disc anodic polarization current (I_d) (b) Ring current (I_r) profiles during one cycle [0.1-1.0] V_{RHE}. (c) Calculated values of S_{H2O2}. (d) S_{H2O2} and I_r maxima vs. disc potential.

The results are summarized in Figure 2 (Au and Pd polycrystals are reported in Figures S4.1-4). The ORR data collected at the disc (I_d in Figure 2a) show at a glance, how the composition significantly affects the ORR onset potentials: from 0.4 V_{RHE} for Au it shifts positively, until 0.9 V_{RHE} for Pd. The theoretical diffusion limited currents (dashed lines in Figure 2a) calculated from the Levich equation [31] suggest a mechanism change from a 2 (dominant H_2O_2 production) to a 4-electrons process with increasing Pd content.

The presence of H_2O_2 is confirmed by the I_r profiles (Figure 2b), corresponding to H_2O_2 oxidation ($H_2O_2 \rightarrow O_2+2H^++2e^-$). The total H_2O_2 current (I_{per}) can be estimated from correcting I_r by the collection efficiency N and compared to I_d (Figure S4.5). As observed from the I_d and the I_r, H_2O_2 production is considerably influenced by composition. In particular, the highest I_r is measured for pure Au (~0.32 mA cm_{geo}^{-2} @0.1 V_{RHE}) and the lowest for Pd (<0.05 mA cm_{geo}^{-2}). Interestingly, for low Pd contents (Au, Au_9Pd, Au_3Pd) the onset potentials at the ring and the disc coincide, while for the remaining composition (AuPd, $AuPd_3$, Pd) the I_r onset potential remains constant at a value close to the standard potential (0.69 V). Note that, in a 2-electron process the peak of the volcano

plot coincides with the standard potential. Thus, a catalyst for the H_2O_2 production can have zero overpotential [32]. Temptatively, the lack of overpotential can explain the fact that the I_r onset potential for active catalyst coincide. Interestingly, for $AuPd_3$ and Pd an I_r peak is observed at low potential (<0.2-0.3 V_{RHE}) where Pd is covered with hydrogen. This is well known also for Pt-based catalysts [33].

As I_r, the S_{H2O2} (Figure 2c) decreases with Pd content from a $S_{H2O2,max}$ of ∼95% to less than 10% for pure Au and Pd respectively. As also observed elsewhere, both S_{H2O2} and I_r exhibit a maximum [7, 8, 13]. Tentatively, this can be attributed to a mechanism change with increasing overpotential. As for the onset-potential also the maxima of I_r and S_{H2O2} are shifting similarly with the composition (Figure 2d). The high S_{H2O2} of Au is confirmed also with poly-Au (see Figure S4.4). Both show similar onset potentials and S_{H2O2} around 95-98%. In a recent publication on carbon supported Au-Pd catalysts, Jirkovsky *et al.* observed a S_{H2O2} enhancement for low Pd concentration (<15%) with a maximum for 8% Pd [7], whose S_{H2O2} approached 95%. This was attributed to geometric effect due the presence of single Pd atoms surrounded by Au. Our Au_9Pd does not show improvement in terms of S_{H2O2} compared to the pure Au sample, whose S_{H2O2} is already approaching 95%. The influence of the support and of isolated Pd needs to be further addressed in future studies. Indeed, first principles calculation suggests an influence on S_{H2O2} due to geometric effect [34], that could correspond to a shift in onset potential while maintaining a high S_{H2O2}.

3.3 Peroxide Reduction and Oxidation Reaction (PROR)

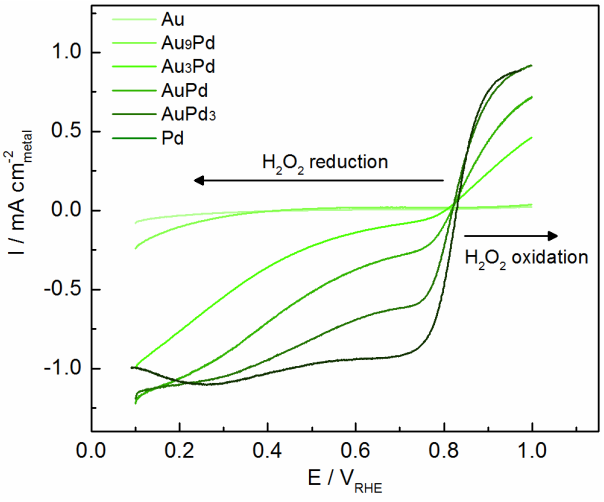

Figure 3 Anodic sweep of the PROR on various Au-Pd catalyst compositions in Ar saturated 0.1M $HClO_4$ + 10mM H_2O_2. Rotation: 900 rpm. Scan rate : 50 mV s^{-1}.

Once produced, H_2O_2 can "degrade" through: (i) electrochemical peroxide reduction (PRR) ($H_2O_2+2e^-+2H^+ \rightarrow 2H_2O$), (ii) electrochemical peroxide oxidation (POR) ($H_2O_2 \rightarrow O_2+2e^-+2H^+$) and (iii) chemical disproportionation ($2H_2O_2 \rightarrow 2H_2O+O_2$). The latter is influenced by the reaction environment, whereas the others are mainly related to the catalyst surface and presence of impurities [35, 36]. It is therefore of utmost importance to answer the question of whether the produced H_2O_2 would be further

reduced in a fuel cell at operational potentials, dominated by PRR. PROR was studied in Ar-saturated 0.1M $HClO_4$ containing 10 mM of H_2O_2 (Figure 3). Interestingly, the polarization curves match around 0.8 V_{RHE}. At such potential, the dominating reaction (PRR to POR) changes with the surface state (reduced to oxidized), as observed for poly-Pt [36]. The Pd oxidation onset is ∼0.7 V_{RHE}, which is indeed when the PRR current starts to decrease (see also poly-Pd in Figure S5.1). Inactive metals for ORR are also less active for PRR: an increase in Au content corresponds to a proportional decrease in both ORR (Figure 2) and PRR (Figure 3). This trend is also confirmed by previous literature on co-electrodeposited Au-Pd [22, 37]. Already at 10% Pd content an undesired (even though limited) increase in the H_2O_2 reduction current was observed. As Au is selective and not active for the PRR, it can be indicated as the best candidate for applications that require high S_{H2O2}.

3.4 Potentiostatic H_2O_2 production

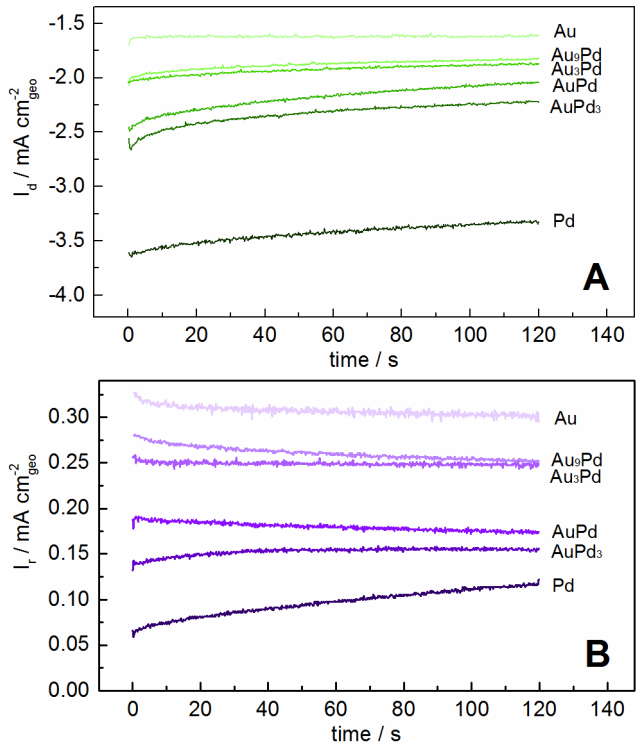

Figure 4 Measured I_d (a) and I_r (b) during 2 min potentiostatic experiment in O_2 saturated 0.1M $HClO_4$. Rotation: 900 rpm. E_d corresponds to the potential of $I_{r,max}$ (see Table 2). Er: 1.28 V_{RHE}.

To finally bridge the gap between possible "real application" and our fundamental studies we need to understand how the catalysts behave during demanding continuous H_2O_2 production. RRDE data (Figure 4 and Figure S6.1) during 2 min potentiostatic condition (potential of $I_{r,max}$ for each composition) confirms the activity and S_{H2O2} trend observed in the previous sections. Interestingly, the I_r (and thus S_{H2O2}) slightly increases with time for Pd rich catalysts ($AuPd_3$, Pd). This is even more evident during the 30 minutes measurements (see Figure S6.1) and can be tentatively attributed to the presence of either impurities or spectator species that initially poison active sites favoring the H_2O_2 production, as observed for Pt [38]. Such spectator species can be

easily removed with a simple CV [13]; indeed, the ORR behavior before and after the measurement is not affected (see Figure S6.2).

The productivity (Table 2) of the catalyst after 2 and 30 minutes is determined from the POR limiting current on Pt (see calibration in Figure S6.3). In line with the high S_{H2O2} and low PRR activity of Au, its productivity is the highest. Thus, the measurement on Au was extended to 1 and 2 h yielding 12.3 and 22.9 mol g_{metal}^{-1} cm^{-2}_{geo}. Increasing the Pd content, the S_{H2O2} decreases and PRR activity increases, resulting in a proportional productivity decrease. Despite the low productivity expected for 4-electron catalysts with low S_{H2O2} as Pd, it yields ∼2.40 mol g_{metal}^{-1} cm^{-2}_{geo} after 30 min. This can be again attributed to a poisoning of the active sites for complete reduction, favoring a 2-electron process.

Table 2 H_2O_2 productivity after 2 and 30 mins of measurement.

	Potential hold (V_{RHE})	Productivity 2 min (mol g_{metal}^{-1} cm^{-2}_{geo})	Productivity 30 min (mol g_{metal}^{-1} cm^{-2}_{geo})
Au	0.10	0.46	6.79
Au_9Pd	0.15	0.39	5.46
Au_3Pd	0.25	0.40	5.87
AuPd	0.40	0.29	3.37
$AuPd_3$	0.45	0.24	3.42
Pd	0. 50	0.14	2.40

4 Conclusions

A set of Au-Pd nanocatalysts are synthesized as model catalysts to study the electrocatalytic behaviour for H_2O_2 synthesis from fundamental perspectives and for continuous H_2O_2 production.

The ORR and the PROR behavior are significantly affected by the composition: upon an increase in Au content we observe an increase in I_r and S_{H2O2}, whereas the onset is shifting to lower potentials. The S_{H2O2} of Au is the highest (95%) at the price of low activity. Previous theoretical studies as well as experimental works suggest that geometrical effects (triggered by the presence of atomically dispersed Pd in Au) might enhance the activity whereas maintaining high S_{H2O2}, which are however not observed in this work. For Au_9Pd and Au_3Pd, the activity is indeed higher (i.e. H_2O_2 formation onset potential already close to nominal for Au_3Pd), but the S_{H2O2} decreases while remaining relatively high (between 60 and 80%). With an eye on applications, these compositions might still be interesting where a compromise between S_{H2O2} and energy output is allowed, as the typical end-user requires H_2O_2 concentration in the range 2-8 wt%. On the other hand, if high H_2O_2 concentration and high S_{H2O2} is required, pure Au would potentially be the catalyst of choice, as the productivity during a potentiostatic measurement indicates (highest productivity that steadily increases up to 2h).

Our observations on a spectrum of compositions between elements with contrasting O_2 adsorption energy can be extended to other alloys with similar characteristic. The

fundamental studies help to forecast the ORR behavior and reaction selectivity for potential applications. Furthermore, future investigations on fuel cells, the stability of catalysts, as well as on the effect of support are of particular importance to understand how these catalysts will perform in real applications.

Acknowledgments

E.P acknowledges financial support from the IMPRS-SurMat doctoral program. O.K. acknowledges financial support from the Alexander von Humboldt Foundation. We thank the MAXNET Energy for the financial support.

References

[1] J.M.Campos-Martin, G.Blanco-Brieva, J.L.G.Fierro, *Hydrogen peroxide synthesis: An outlook beyond the anthraquinone process*, Angew Chem Int Edit, 45 (2006) 6962-6984.

[2] J.K.Edwards, S.J.Freakley, R.J.Lewis, J.C.Pritchard, G.J.Hutchings, *Advances in the direct synthesis of hydrogen peroxide from hydrogen and oxygen*, Catal Today, 248 (2015) 3-9.

[3] H.Riedl, G.Pfleiderer, *Production of hydrogen peroxide*. US Patent 2158525, (1939).

[4] J.K.Edwards, B.Solsona, E.N.N, A.F.Carley, A.A.Herzing, C.J.Kiely, G.J.Hutchings, *Switching Off Hydrogen Peroxide Hydrogenation in the Direct Synthesis Process*, Science, 323 (2009) 1037-1041.

[5] E.Brillas, F.Alcaide, P.L.Cabot, *A small-scale flow alkaline fuel cell for on-site production of hydrogen peroxide*, Electrochim Acta, 48 (2002) 331-340.

[6] I.Yamanaka, T.Onisawa, T.Hashimoto, T.Murayama, *A Fuel-Cell Reactor for the Direct Synthesis of Hydrogen Peroxide Alkaline Solutions from H_2 and O_2*, Chemsuschem, 4 (2011) 494-501.

[7] J.S.Jirkovsky, I.Panas, E.Ahlberg, M.Halasa, S.Romani, D.J.Schiffrin, *Single Atom Hot-Spots at Au-Pd Nanoalloys for Electrocatalytic H_2O_2 Production*, J Am Chem Soc, 133 (2011) 19432-19441.

[8] S.Siahrostami, A.Verdaguer-Casadevall, M.Karamad, D.Deiana, P.Malacrida, B.Wickman, M.Escudero-Escribano, E.A.Paoli, R.Frydendal, T.W.Hansen, I.Chorkendorff, I.E.L.Stephens, J.Rossmeisl, *Enabling direct H_2O_2 production through rational electrocatalyst design*, Nat Mater, 12 (2013) 1137-1143.

[9] I.Yamanaka, T.Onizawa, S.Takenaka, K.Otsuka, *Direct and Continuous Production of Hydrogen Peroxide with 93% Selectivity Using a Fuel-Cell System*, Angew Chem Int Edit, 42 (2003) 3653-3655.

[10] F.R.Duke, T.W.Haas, *Homogeneous Base-Catalyzed Decomposition of Hydrogen Peroxide*, J Phys Chem-Us, 65 (1961) 304-&.

[11] H.S.Wroblowa, Y.C.Pan, G.Razumney, *Electroreduction of Oxygen: A New Mechanistic Criterion*, J Electroanal Chem, 69 (1976) 195-201.

[12] C.H.Choi, H.C.Kwon, S.Yook, H.Shin, H.Kim, M.Choi, *Hydrogen Peroxide Synthesis via Enhanced Two-Electron Oxygen Reduction Pathway on Carbon-Coated Pt Surface*, J Phys Chem C, 118 (2014) 30063-30070.

[13] A.Verdaguer-Casadevall, D.Deiana, M.Karamad, S.Siahrostami, P.Malacrida, T.W.Hansen, J.Rossmeisl, I.Chorkendorff, I.E.L.Stephens, *Trends in the Electrochemical Synthesis of H_2O_2: Enhancing Activity and Selectivity by Electrocatalytic Site Engineering*, Nano Lett, 14 (2014) 1603-1608.

[14] S.Cherevko, A.A.Topalov, I.Katsounaros, K.J.J.Mayrhofer, *Electrochemical dissolution of gold in acidic medium*, Electrochem Commun, 28 (2013) 44-46.

[15] J.K.Edwards, S.J.Freakley, A.F.Carley, C.J.Kiely, G.J.Hutchings, *Strategies for Designing Supported Gold–Palladium Bimetallic Catalysts for the Direct Synthesis of Hydrogen Peroxide*, Accounts of Chemical Research, 47 (2014) 845-854.

[16] M.Shao, *Palladium-based electrocatalysts for hydrogen oxidation and oxygen reduction reactions*, J Power Sources, 196 (2011) 2433-2444.

[17] P.Rodriguez, M.T.M.Koper, *Electrocatalysis on gold*, Phys Chem Chem Phys, 16 (2014) 13583-13594.

[18] S.Strbac, N.A.Anastasijevic, R.R.Adzic, *Oxygen Reduction on Au(100) and Vicinal Au(910) and Au(11, 1, 1) Faces in Alkaline-Solution: a Rotating-Disk Ring Study*, J Electroanal Chem, 323 (1992) 179-195.

[19] N.M.Markovic, R.R.Adzic, V.B.Vesovic, *Structural Effects in Electrocatalysis: Oxygen Reduction on the Gold Single-Crystal Electrodes with (110) and (111) Orientations*, J Electroanal Chem, 165 (1984) 121-133.

[20] C.M.Sanchez-Sanchez, A.J.Bard, *Hydrogen Peroxide Production in the Oxygen Reduction Reaction at Different Electrocatalysts as Quantified by Scanning Electrochemical Microscopy*, Anal Chem, 81 (2009) 8094-8100.

[21] J.S.Jirkovsky, I.Panas, S.Romani, E.Ahlberg, D.J.Schiffrin, *Potential-Dependent Structural Memory Effects in Au-Pd Nanoalloys*, J Phys Chem Lett, 3 (2012) 315-321.

[22] H.Erikson, A.Sarapuu, J.Kozlova, L.Matisen, V.Sammelselg, K.Tammeveski, *Oxygen Electroreduction on Electrodeposited PdAu Nanoalloys*, Electrocatalysis-Us, 6 (2015) 77-85.

[23] F.Maroun, F.Ozanam, O.M.Magnussen, R.J.Behm, *The role of atomic ensembles in the reactivity of bimetallic electrocatalysts*, Science, 293 (2001) 1811-1814.

[24] J.Pritchard, L.Kesavan, M.Piccinini, Q.He, R.Tiruvalam, N.Dimitratos, J.A.Lopez-Sanchez, A.F.Carley, J.K.Edwards, C.J.Kiely, G.J.Hutchings, *Direct Synthesis of Hydrogen Peroxide and Benzyl Alcohol Oxidation Using Au-Pd Catalysts Prepared by Sol Immobilization*, Langmuir, 26 (2010) 16568-16577.

[25] Z.J.Li, F.Gao, Y.L.Wang, F.Calaza, L.Burkholder, W.T.Tysoe, *Formation and characterization of Au/Pd surface alloys on Pd(111)*, Surf Sci, 601 (2007) 1898-1908.

[26] S.Cherevko, A.A.Topalov, A.R.Zeradjanin, I.Katsounaros, K.J.J.Mayrhofer, *Gold dissolution: towards understanding of noble metal corrosion*, Rsc Adv, 3 (2013) 16516-16527.

[27] M.Lukaszewski, K.Kusmierczyk, J.Kotowski, H.Siwek, A.Czerwinski, *Electrosorption of hydrogen into palladium-gold alloys*, J Solid State Electr, 7 (2003) 69-76.

[28] M.Lukaszewski, A.Czerwinski, *Electrochemical behavior of palladium-gold alloys*, Electrochim Acta, 48 (2003) 2435-2445.

[29] D.A.J.Rand, R.Woods, *Determination of Surface Composition of Smooth Noble-Metal Alloys by Cyclic Voltammetry*, J Electroanal Chem, 36 (1972) 57-69.

[30] K.Gossner, E.Mizera, *The Anodic Oxidation of Gold+Palladium Alloys*, J Electroanal Chem, 140 (1982) 47-56.

[31] A.J.Bard, L.R.Faulkner, *Electrochemical Methods*, Wiley, New York, 2nd edition (2001).

[32] S.Siahrostami, A.Verdaguer-Casdevall, M.Karamad, I.Chorkendorff, I.Stephens, J.Rossmeisl, *Activity and Selectivity for O_2 Reduction to H_2O_2 on Transition Metal Surfaces*, ECS Transactions, 58 (2013) 53-62.

[33] N.M.Markovic, H.A.Gasteiger, P.N.Ross, *Oxygen Reduction on Platinum Low-Index Single-Crystal Surfaces in Sulfuric-Acid-Solution: Rotating Ring-Pt(Hkl) Disk Studies*, J Phys Chem-Us, 99 (1995) 3411-3415.

[34] H.C.Ham, G.S.Hwang, J.Han, S.W.Nam, T.H.Lim, *Geometric Parameter Effects on Ensemble Contributions to Catalysis: H_2O_2 Formation from H_2 and O_2 on AuPd Alloys. A First Principles Study*, J Phys Chem C, 114 (2010) 14922-14928.

[35] I.Katsounaros, J.C.Meier, K.J.J.Mayrhofer, *The impact of chloride ions and the catalyst loading on the reduction of H_2O_2 on high-surface-area platinum catalysts*, Electrochim Acta, 110 (2013) 790-795.

[36] I.Katsounaros, W.B.Schneider, J.C.Meier, U.Benedikt, P.U.Biedermann, A.A.Auer, K.J.J.Mayrhofer, *Hydrogen peroxide electrochemistry on platinum: towards understanding the oxygen reduction reaction mechanism*, Phys Chem Chem Phys, 14 (2012) 7384-7391.

[37] T.C.Nagaiah, D.Schafer, W.Schuhmann, N.Dimcheva, *Electrochemically Deposited Pd-Pt and Pd-Au Codeposits on Graphite Electrodes for Electrocatalytic H_2O_2 Reduction*, Anal Chem, 85 (2013) 7897-7903.

[38] I.Katsounaros, W.B.Schneider, J.C.Meier, U.Benedikt, P.U.Biedermann, A.Cuesta, A.A.Auer, K.J.J.Mayrhofer, *The impact of spectator species on the interaction of H_2O_2 with platinum - implications for the oxygen reduction reaction pathways*, Phys Chem Chem Phys, 15 (2013) 8058-8068.